JOURNAL OF PROPULSION AND POWER
Vol. 17, No. 3, May–June 2001

Manipulation of Shock/Boundary-Layer Interactions in Hypersonic Inlets

D. Schulte,* A. Henckels,† and R. Neubacher†
DLR, German Aerospace Research Center, 51147 Cologne, Germany

The possibilities of manipulating shock/boundary-layer interactions are demonstrated with regard to an application for hypersonic inlets. Experiments on generic models have been carried out in the hypersonic wind tunnel of the German Aerospace Research Center at Mach 6 and laminar flow conditions. Experimental results were validated by numerical flow simulations using a two-dimensional finite element scheme. In the case of shock-induced boundary-layer separation, it could be shown that the implementation of bleed leads to a reduction of the separation bubble thickness by almost 50%. Further experimental investigations dealt with the achievable reduction of the heat loads on the wall surface depending on the amount and the position of the boundary-layer bleed. These examinations were extended to three-dimensional corner flows and favorable design parameters for a boundary-layer bleed setup were found. Finally, the results obtained using the generic models were transferred to a hypersonic inlet model. There the application of a correctly designed and positioned bleed system showed a significant increase of the attainable total pressure recovery.

Nomenclature

B_A	=	bleed slot width
c_f	=	skin-friction coefficient
H	=	effective inlet height
h^*	=	height of the internal cross section
L_A	=	length of the bleed slot
l	=	model length
M	=	Mach number
$\dot{m}$	=	mass flow rate
Re	=	Reynolds number
St	=	Stanton number
v	=	velocity
x, y	=	coordinates
β	=	turning angle of the flow (angle of the shock generator wedge)
γ_A	=	bleed slot angle
Δx_{AS}	=	distance of the bleed slot from the shock impingement position
δ	=	boundary-layer thickness
δ^*	=	displacement thickness

Subscripts

A	=	bleed
G	=	undisturbed boundary layer at the shock impingement location
∞	=	freestream conditions

Introduction

FOR the design of future hypersonic space transportation planes, airbreathing propulsion is one of the key technologies. The inlet particularly is of great importance for the efficiency of the propulsion system and, therefore, for the maximal attainable payload of the whole transportation plane.

In hypersonic inlets, viscous effects have an important influence on the inlet flowfield and, by this, on the efficiency of the inlet system. One of the dominating flow phenomena in a hypersonic inlet is the interaction of oblique shocks induced by the inlet ramps with the boundary layer developing on the inlet walls.

Figure 1, the result of a numerical simulation using a finite element method on unstructured, adaptive meshes,[1] shows the important viscous effects occurring in an inlet. For the simulation, a generic two-dimensional multiple ramp model has been used to determine the regions where shock/boundary-layer interactions may result in losses of the inlet efficiency.

At the front tip of the ramp, the formation of the boundary layer leads to a displacement of the induced ramp shock (detail in lower left corner). The impingement of an oblique shock on a boundary layer can result in a boundary-layer separation (see detailed view in upper right corner). Depending on the flow conditions, that is, Mach and Reynolds numbers, and on the given geometry, the boundary layer may also separate at a wedge formed by adjacent ramps (as shown in the detail in the lower right corner).

This paper will focus on two of these effects, that is, the boundary-layer separation caused by an impinging shock and the boundary-layer separation at compression ramps. These flow phenomena may have a double influence on the flow inside an inlet. First, boundary-layer separations reduce the effective flow surface because they represent a considerable low-energy mass flow. Second, they can induce high local heat loads on the inlet walls due to the development of longitudinal vortices.

The objective of the examinations presented here is to improve the inlet efficiency by finding effective measures to manipulate shock/boundary-layer interactions. In previous investigations,[2,3] boundary-layer bleed has been identified as one of the most powerful methods to reduce boundary-layer separations. In this paper, the application of boundary-layer bleed for the improvement of the inlet efficiency will be demonstrated.

Experimental Setup

The experiments presented have been carried out in the German Aerospace Research Center hypersonic blow-down wind-tunnel facility. Using different Laval nozzles, Mach numbers ranging from 4.8 to 11.2 can be realized with a test duration of about 40 s. Depending on the ambient flow conditions, Reynolds numbers of up to 20×10^6/m can be reached.

As diagnostic tools, the facility offers a schlieren visualization and an advanced focal plane array (FPA) infrared system for the measurement of temperatures on the model surface (Fig. 2). When locally one-dimensional heat transfer is assumed, the heat fluxes can be calculated from the time history of the measured temperature.

Received 16 October 1999; revision received 11 May 2000; accepted for publication 4 December 2000.

*Research Engineer; currently at Valeo Electrical Systems, Simulation Department, 2 rue André Boulle, 94017 Créteil, France.
†Research Engineer, Institute of Fluid Mechanics, Wind Tunnel Division.

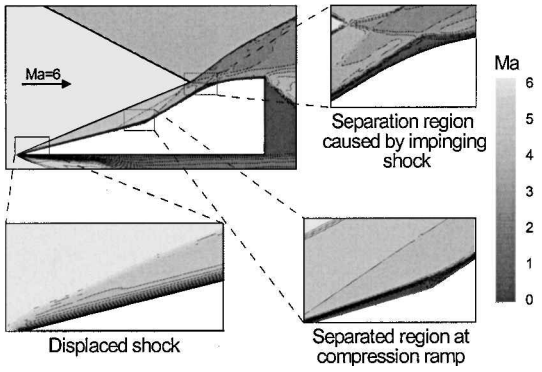

Fig. 1 Viscous effects in hypersonic inlet flow.

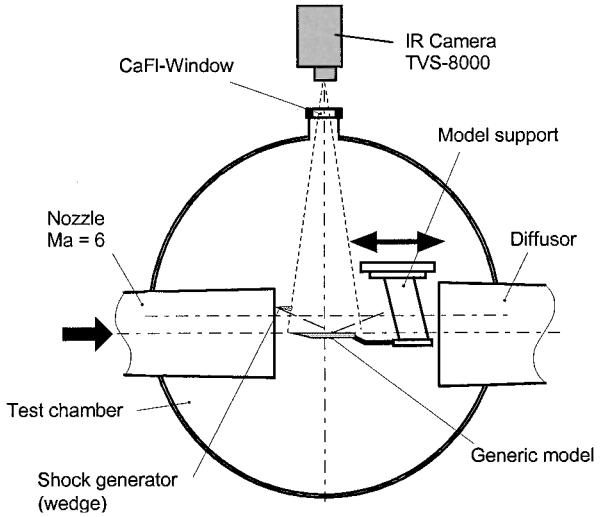

Fig. 2 Hypersonic wind-tunnel facility with a mounted generic model.

Most of the experiments were carried out employing generic models that are designed with the aid of computational simulations.[3] The use of such models permits focusing the investigations on the key phenomena of inlet flow. The common basis of these models is a flat-plate model equipped with a planar bleed slot (as shown in Fig. 3) to investigate the influence of mass flow suction (bleed) on boundary-layer separations.

This separation is induced by an oblique shock that is generated by a shock generator (Fig. 2). The generic model can be equipped with various means to manipulate shock/boundary-layer interactions. The model consists of several Teflon® plates embedded in a metal frame, which can be easily exchanged and adjusted to obtain various bleed geometries, that is, different bleed slot angles γ_A and slot widths B_A.

Based on this geometry, a side wall can be fixed to the generic model to examine the efficiency of the bleed slot configuration in three-dimensional flows. To investigate shock/boundary-layer interactions of ramp flows, a compression ramp featuring a variable bleed slot can be added to the generic model.

Manipulation of Shock/Boundary-Layer Interactions

Implementation of Boundary-Layer Bleed

A generic model configuration (Fig. 3) has been designed (using an analytical design method[2]) and tested in the German Aerospace Research Center hypersonic wind tunnel facility. To obtain significant shock/boundary-layer interactions, laminar conditions at a freestream Mach number of $M_\infty = 6$ and a freestream Reynolds number of $Re_\infty = 4 \times 10^6$/m have been chosen.

One method to visualize the effects of boundary-layer bleed at hypersonic flow conditions is the use of schlieren photography. In

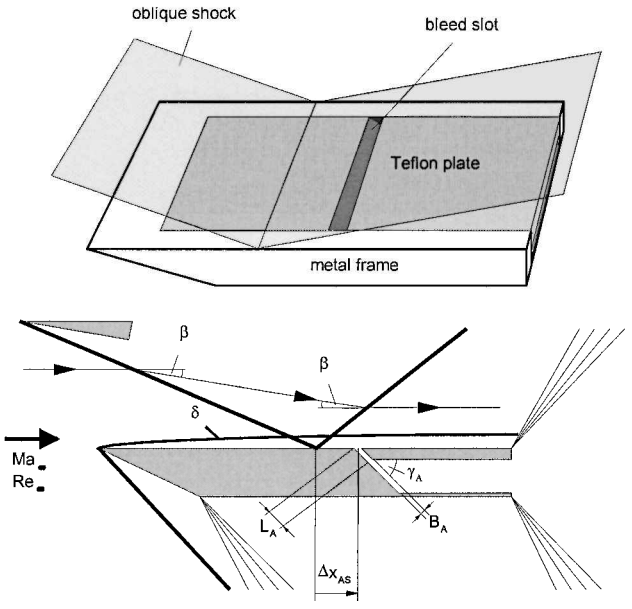

Fig. 3 Generic flat plate base model with planar bleed slot.

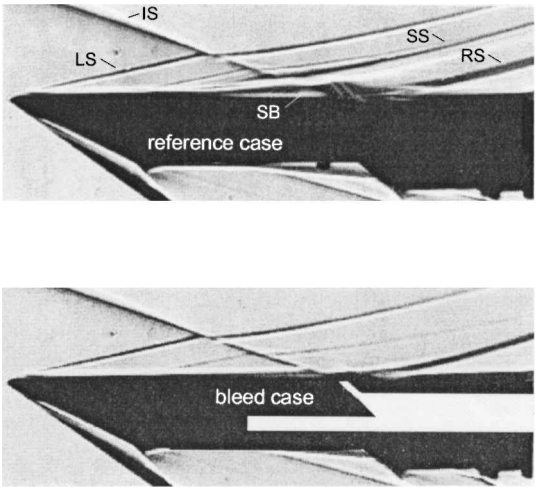

Fig. 4 Flowfield for the reference case and a case with optimized bleed: $M_\infty = 6$ and $Re_\infty = 4 \times 10^6$/m.

Fig. 4, schlieren pictures for a reference case without bleed and a case with optimized bleed setup (described subsequently) are displayed.

The impinging shock (IS), induced by a shock generator, interacts with the leading-edge shock (LS) of the model, which slightly changes its angle. Downstream of the shock impingement point, a reattachment shock (RS) is visible. For the reference case, the impingement of the oblique shock forms a separation bubble (SB) on the model surface. The existence of this separation region induces an additional shock, the so-called separation shock (SS). Note that the implementation of an optimized boundary-layer bleed effectively prevents the occurrence of a boundary-layer separation. Further proof for this is the nonexistence of the separation shock.

The effectiveness of the boundary-layer bleed is confirmed by the results of numerical simulations using the finite element solver mentioned earlier. Figure 5 shows the results of these simulations as Mach number distributions. Complementary to the flowfield on the model surface, the numerical simulation delivers information about the flow inside the bleed slot. For example, with the help of the numerical simulation, it can be proven that the flow through the bleed slot is critical for the chosen test conditions.

In a first model setup, a long bleed slot length L_A has been used (Mach number distribution in the middle of Fig. 5). When the length

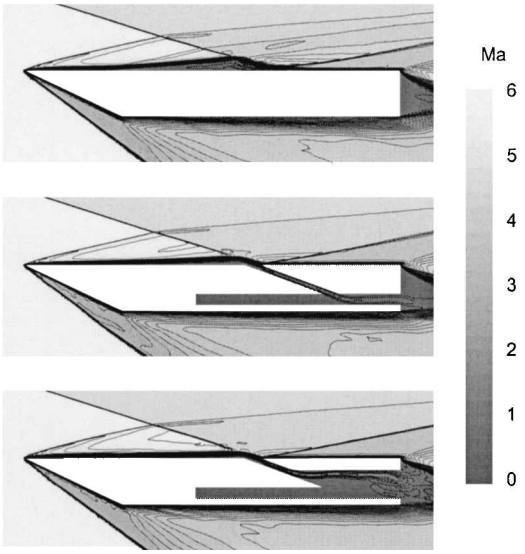

Fig. 5 Calculated Mach number contours for the reference case, a first bleed slot setup and the optimized bleed configuration $M_\infty = 6$ and $Re_\infty = 4 \times 10^6$/m.

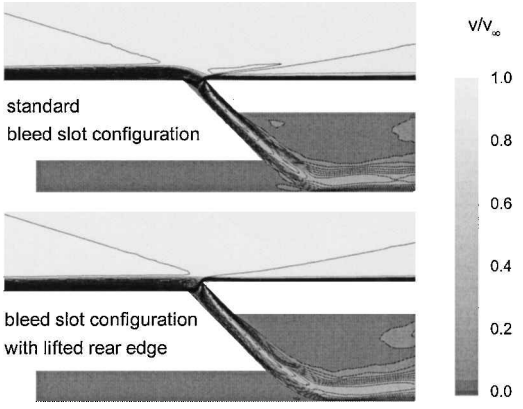

Fig. 6 Calculated velocity contours for the standard bleed slot setup and a bleed slot configuration with lifted rear edge: $M_\infty = 6$ and $Re_\infty = 4 \times 10^6$/m.

of the bleed slot (reduction of the plate thickness of the second part of the Teflon plate, Fig. 3), is reduced, the flow inside the bleed slot can be improved significantly. The Mach number distribution visible in the lower part of Fig. 5 shows that the thickness of the boundary layers in the bleed slot has decreased; the flow has already become critical at the beginning of the bleed slot. Furthermore, the acceleration of the flow inside the bleed slot is higher for this setup, thus, increasing the effectiveness of the boundary-layer bleed.

When the downstream edge of the bleed slot is lifted slightly, the efficiency of the boundary-layer bleed can be further improved. In this case, the rear edge of the bleed slot should be about δ_G, where δ_G is the thickness of the undisturbed boundary layer at the location of the impinging oblique shock, higher than the first part of the model surface. Figure 6 shows the calculated velocity (normalized with the freestream velocity) in the vicinity of the bleed slot for a standard bleed setup (upper part of Fig. 6) and a bleed setup with a lifted rear edge (lower part of Fig. 6). It can be seen that almost the complete boundary layer is drawn away by the boundary-layer bleed for the setup with a lifted rear bleed slot edge, and a new, undisturbed boundary layer is formed downstream of the bleed slot. On the other hand, this bleed slot configuration also significantly increases the amount of bleed mass flow, which may be not desired for certain applications. Therefore, lifting the rear edge of the bleed slot may be a solution for critical configurations where a maximum boundary-layer control is needed.

In Fig. 7, a comparison of the skin-friction coefficient c_f for the reference case and the case with boundary-layer bleed is shown. A

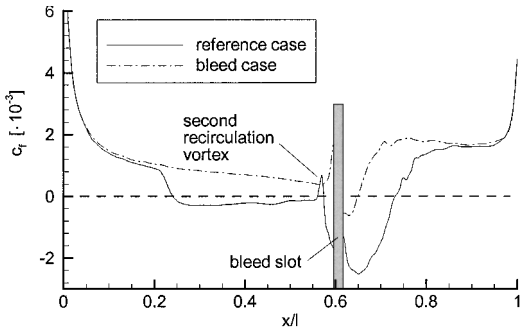

Fig. 7 Calculated skin-friction coefficient for the reference case and the optimized bleed setup.

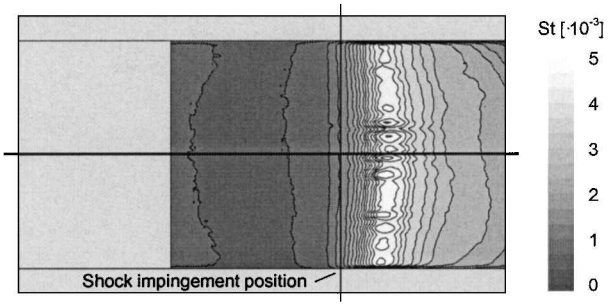

Fig. 8 Measured Stanton number contours on the model surface for the reference case: $M_\infty = 6$ and $Re_\infty = 4 \times 10^6$/m.

big separation bubble can be noticed for the reference case (values of the skin-friction coefficient less then zero indicate boundary-layer separation). Additionally, a second recirculation vortex, which has already been observed in former investigations,[4] is recognizable by the peak of c_f marked in the diagram. For the case with boundary-layer bleed, the boundary-layer separation has almost completely vanished (values of c_f almost always greater than zero).

It has been previously shown[2] that the slot width B_A and the slot angle γ_A are the main parameters of influence for the bleed flow. For the given laminar flow conditions, the bleed slot should have a width of about $1.5 \times \delta_G$. When the bleed slot angle is considered, a compromise between a short slot length (the plate thickness is supposed to be fixed) and a smooth turning of the flow inside the bleed slot should be sought. Therefore, a bleed slot angle of about 45 deg has been found to be favorable. These optimized parameters for the bleed slot setup have, thus, been used for the results presented earlier.

Another important parameter of influence for the boundary-layer bleed is the position of the bleed slot relative to the shock impingement position. Former experiments[3] have yielded a position of the bleed slot in the direct vicinity of the shock impingement position as the most favorable. More precisely, a position directly upstream of the impinging shock (which means that the bleed slot is positioned in front of the shock impingement location) results additionally in the lowest bleed mass flow necessary for an efficient function of the boundary-layer bleed. In this case, the maximum distance between the center of the bleed slot and the impinging shock should not be greater than double the boundary-layer thickness δ_G. Note that a low bleed mass flow is desirable for the implementation of boundary-layer bleed in hypersonic inlets because for this configuration less mass flow is drawn away by the boundary-layer bleed, therefore granting a high inlet mass flow.

For the reference case, downstream of the separation region, the reattachment of the separated shear layer induces high levels of heat transfer on the model surface. Because of the concave curvature of the separation bubble, Görtler vortices develop downstream of the shock impingement location. The distribution of the Stanton numbers on the model surface, derived from the infrared thermography, shows (Fig. 8) that these vortices cause a spanwise modulation of the thermal loads on the model wall.[5]

The structure of the vortices can be displayed using oil film visualization. The oil spread on the model surface is distributed by the

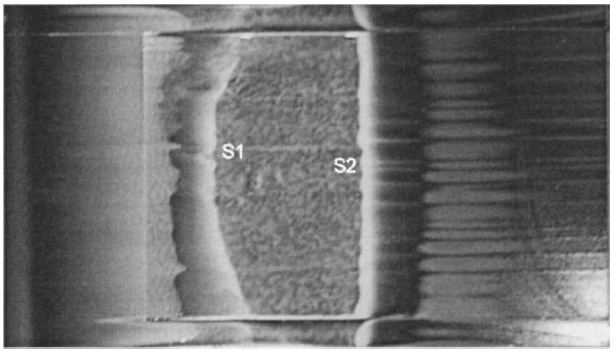

Fig. 9 Visualization of the wall shear stresses for the reference case.

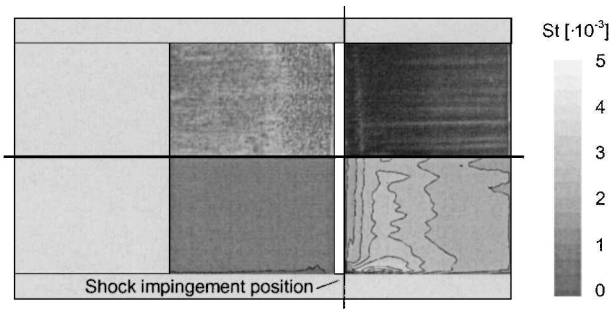

Fig. 10 Wall shear stresses (upper half) and Stanton number contours (lower half) for the case with bleed: $M_\infty = 6$ and $Re_\infty = 4 \times 10^6$/m.

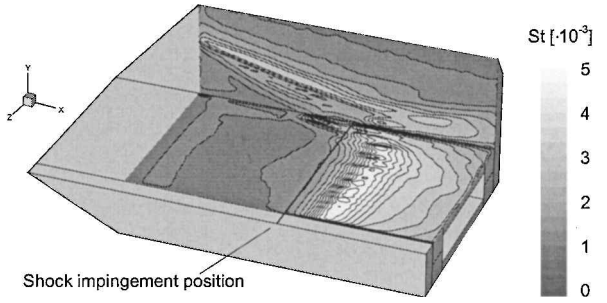

Fig. 11 Stanton number contours on the model plate and the model side wall for the reference case: $M_\infty = 6$ and $Re_\infty = 4 \times 10^6$/m.

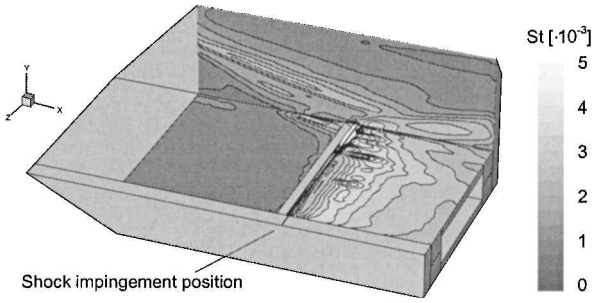

Fig. 12 Stanton number contours on the model plate and the model side wall for the case with bleed: $M_\infty = 6$ and $Re_\infty = 4 \times 10^6$/m.

shear forces that are caused by the flowfield. Because of the Görtler vortices, streamwise striations can be recognized in Fig. 9, downstream of the shock impingement location. Furthermore, the separation line S1, which marks the beginning of the separation region, is visible. In former studies,[4] the occurrence of a second separation line S2 could have been proven. Underneath the shock-induced separation bubble, a second recirculation region, rotating counterwise, is formed. The existence of this second recirculation vortex has also been shown in numerical simulations as described earlier (Fig. 7).

The high thermal loads on the wall surface, as demonstrated in Fig. 8, explain the necessity of effectively reducing the effects of shock/boundary-layer interactions. When the bleed setup already used in Figs. 4 and 5 is used, it can be shown that the boundary-layer bleed is not only valuable for the reduction of the separation bubble, but also, as these effects are combined, for a reduction of heat loads on the model surface. Figure 10 shows (lower-half) the thermal loads on the model with implemented boundary-layer bleed. In the upper-half of Fig. 10, it can be seen that the striation pattern due to the occurrence of Görtler vortices (Fig. 9) has also almost completely vanished.

Three-Dimensional Flowfield with Boundary-Layer Bleed

The investigations presented have been made using a planar model, reducing the flowfield to an almost two-dimensional one. Nevertheless, the flowfield inside a hypersonic inlet is strongly three-dimensional because the side walls of the inlet may play an important role for the structure of the flowfield and, thus, for the interactions between shocks and boundary layers. Therefore, the generic model has been equipped with one side wall to examine the influence of a three-dimensional flow on the function of the boundary-layer bleed.

As the chosen model setup for the investigations of the three-dimensional flow does not feature transparent side walls, visualization of the flow by schlieren photography is not possible. Furthermore, a two-dimensional visualization method such as schlieren photography does not deliver satisfying results for a three dimensionally highly complex flowfield. It has been shown earlier, however, that the effects of the shock-induced boundary-layer separation and the thermal loads on the model surface are strongly linked to each other. For this reason, the studies concerning the three-dimensional flow are focused on the analysis of the heat loads on the model walls.

In Fig. 11, the Stanton number distribution on the generic model is displayed for the reference case, that is, without manipulation of the shock/boundary-layer interactions. The striation pattern that has been observed for the two-dimensional generic model can also be seen for the three-dimensional flow. On the side wall, the impinging shock modulates a characteristic pattern with a maximum heat load along the location of the oblique shock. Because of the interaction of the shocks from the leading edge of the plate and the side wall and the impinging shock with the boundary layer,[6] a separation region is visible upstream of the shock impingement position directly in the edge between the plate and the side wall. In this separation region, the heat loads downstream of the shock impingement position are lower compared to those that occur due to the Görtler vortices.

Similar to the two-dimensional flow, the implementation of boundary-layer bleed leads to a strong reduction of the vortex-induced thermal loads on the plate surface. Figure 12 shows for an optimized bleed setup that the formation of the characteristic striation pattern is strongly diminished by employing boundary-layer bleed.

Nevertheless, a region with high local thermal loads can be observed at the rear edge of the bleed slot in the direct vicinity of the edge between the plate and the side wall. In this region, the thermal loads are even higher than for the reference case. Apparently, the boundary-layer bleed is not able to reduce the separation region in the model edge. Moreover, the turning of the mass flow into the slot induces high local thermal loads at the bleed slot's rear edge (representing a stagnation point for the arriving boundary-layer flow). To prevent this intense heating, the bleed slot should not begin directly at the model's edge but in a certain distance to it (depending on the boundary-layer thickness in the shock impingement region).

Boundary-Layer Separation at Compression Ramps

As demonstrated in the introduction (Fig. 1), the flow over a compression ramp may lead to a separation of the boundary layer.[7] To examine the flow over such a compression ramp, similar to those in hypersonic inlets, the generic model has been equipped with a ramp module featuring a ramp angle of 15 deg. Different from the experiments presented earlier, the chosen flow conditions are $M_\infty = 5.3$ and $Re_\infty = 4.2 \times 10^6$/m.

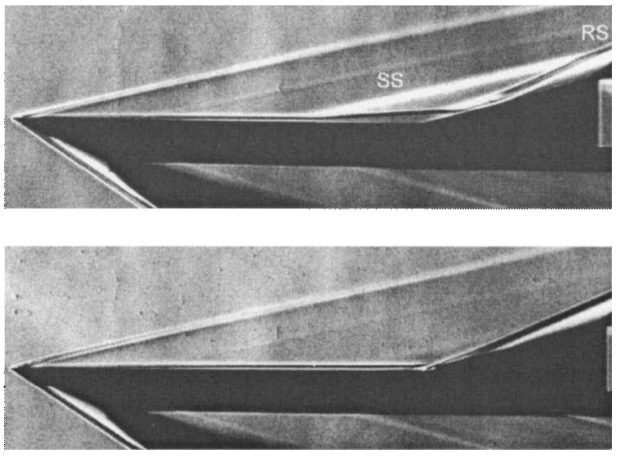

Fig. 13 Ramp flow for a reference case and a case with optimized bleed shown using schlieren visualization: $M_\infty = 5.3$ and $Re_\infty = 4.2 \times 10^6$/m.

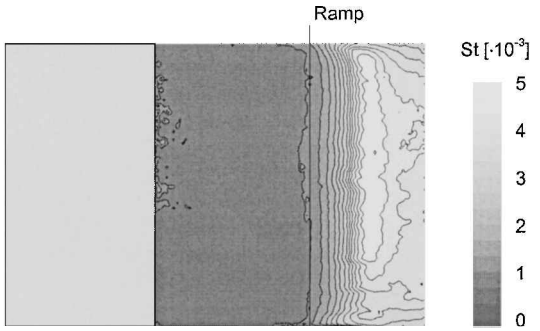

Fig. 14 Measured Stanton number contours on the generic ramp model for the reference case: $M_\infty = 5.3$ and $Re_\infty = 4.2 \times 10^6$/m.

In Fig. 13, schlieren photographs obtained for the ramp flow are shown. The upper part of Fig. 13 shows the reference case without manipulation of the shock/boundary-layer interactions. In an inviscid consideration of the ramp flow, only one shock exists directly at the beginning of the ramp. This ramp shock is caused by the turning of the flow at the ramp, and its angle corresponds to the ramp angle. In contrast to this, the schlieren photography shows the occurrence of a big SB located in the vicinity of the ramp, which begins a large distance upstream of the ramp. Because of the existence of this boundary-layer separation, two shocks are induced: an SS at the beginning of the SB and an RS at the reattachment location of the boundary-layer separation. Farther downstream, these two shocks join each other and form one single shock.

The implementation of a boundary-layer bleed slot directly at the beginning of the ramp almost completely prevents the development of a separation bubble (see lower schlieren photograph in Fig. 13). That is why only one single ramp shock, induced by the ramp angle, can be recognized for the case with boundary-layer bleed.

The occurrence of a boundary-layer separation for the reference case leads to high local thermal loads on the ramp part of the generic model wall (see Fig. 14). Furthermore, the concave curvature of the separation bubble induces, similar to the planar generic model with shock/boundary-layer interaction (Fig. 8), Görtler vortices downstream of the reattachment location of the boundary-layer separation. These vortices increase the heat load on the ramp wall further.

A bleed slot implemented directly at the beginning of the ramp is not only effective for the reduction of the boundary layer (Fig. 13), but is, by this, also able to diminish the thermal loads on the ramp wall downstream of the ramp shock. In the infrared thermography shown in Fig. 15, local hot spots at the rear edge of the bleed slot, that is, at the beginning of the ramp, can be recognized. These locations with higher heat load are due to the turning of the flow into the bleed slot, transforming the bleed slot's rear edge to a stagnation point for the boundary-layer flow.

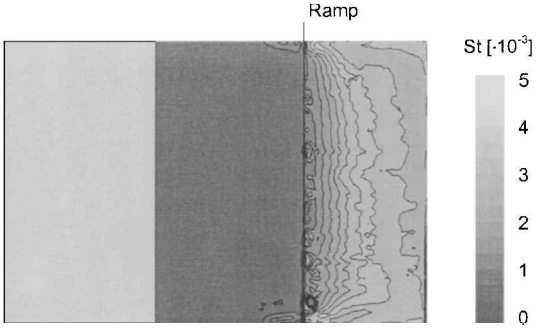

Fig. 15 Measured Stanton number contours on the generic ramp model for the case with bleed: $M_\infty = 5.3$ and $Re_\infty = 4.2 \times 10^6$/m.

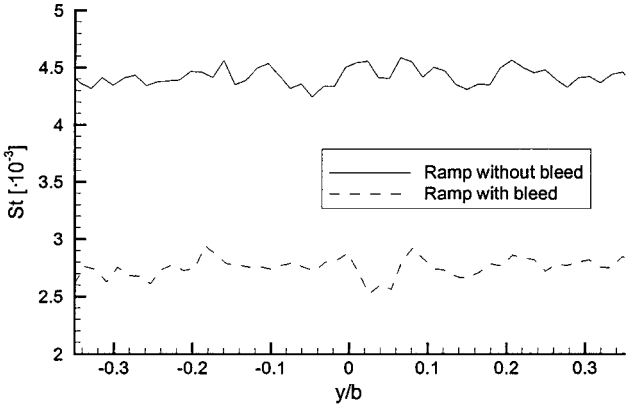

Fig. 16 Comparison of the Stanton numbers crosswise to the freestream flow direction for the reference case and a case with bleed.

Nevertheless, the implemented boundary-layer bleed proves to be very effective for a reduction of thermal loads caused by separation-induced vortices (as, for example, Görtler vortices). Figure 16 shows the measured Stanton numbers crosswise to the freestream flow direction at the position where, for the reference case, the maximum heat loads occur. It can be seen that a reduction of about 40% regarding the thermal load (compared to the reference case without bleed) can be achieved by implementing a boundary-layer bleed.

Note that, regardless of the high benefit of boundary-layer bleed, an implementation of a bleed slot directly in front of a ramp inside a hypersonic inlet may be difficult because the ramps in those inlet systems are often designed to be variable to adapt to different inflow conditions (see the subsequent description of the German Aerospace Research Center hypersonic inlet model). Therefore, the implementation of bleed for the reduction of boundary-layer bleed in the direct vicinity of compression ramps in hypersonic inlets may in some cases be limited to inlet types with fixed geometry.

Generic Hypersonic Inlet

The fundamental investigations regarding methods to influence shock/boundary-layer interactions have been carried out using generic models to isolate one single shock/boundary-layer interaction. Now, the results of these examinations will be transferred to a hypersonic inlet model. For this purpose, a hypersonic inlet model (see Fig. 17), developed at the German Aerospace Research Center, has been equipped with boundary-layer bleed at different locations.

This inlet model is designed for a freestream Mach number of $M_\infty = 5.3$. It is equipped with a pivoting second compression ramp allowing change of the second ramp angle. By this, the height of the internal cross section h^* can be varied to adapt the inlet system to varying inflow conditions as well as to start the model in the wind tunnel. The effective inlet height is $H = 100$ mm, leading to a flow capture area of 10^4 mm^2. In the detail in Fig. 17, an enlargement of an implemented bleed slot can be seen. For a variation of the exit pressure, a hydraulic throttle is used at the inlet exit.

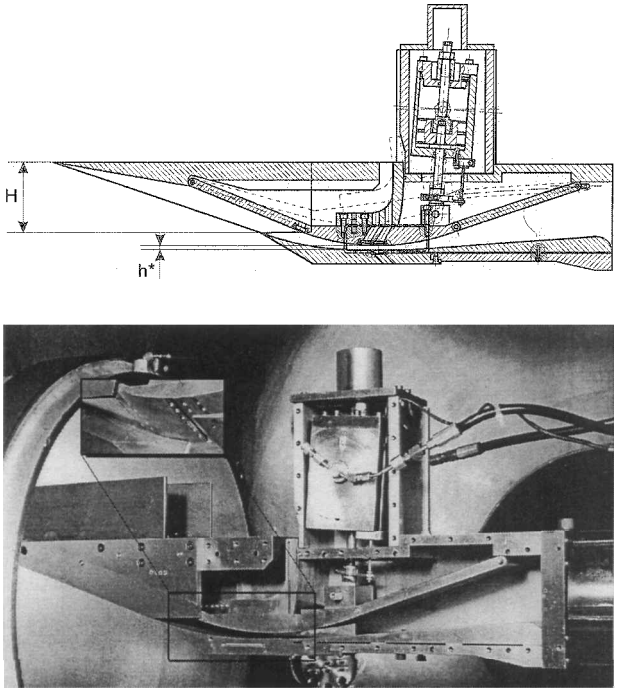

Fig. 17 Sketch and photograph (with partially removed side wall) of the DLR hypersonic inlet model S02A.

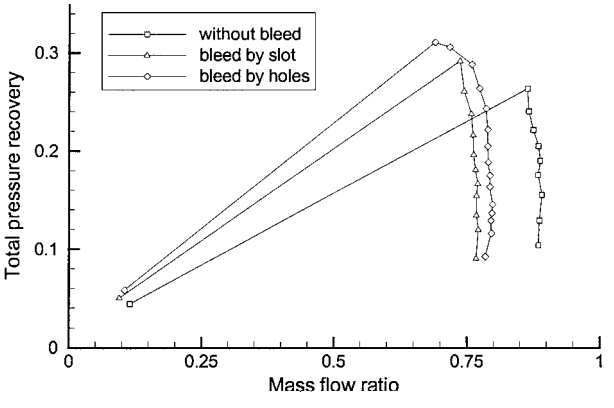

Fig. 18 Comparison of the throttle curves for the DLR inlet model S02A without bleed and with different bleed configurations.

Figure 18 shows a comparison of the throttle curves for the German Aerospace Research Center hypersonic inlet model without bleed and with different bleed configurations at the optimal height of the internal cross section h^*. The mass flow rate is referred on the inviscid inlet flow without spillage and bleed.

When the exit pressure is increased, the total pressure recovery (i.e., the relation of the total pressure at the inlet exit to the total pressure of the incoming flow) is raised, too. At a certain exit pressure, the flow through the inlet becomes choked, leading to a collapse of the inlet flow. For the reference case without bleed, the mass flow ratio (i.e., the relation of the mass flow at the inlet exit to the mass flow at the inlet entrance) remains almost constant.

By the implementation of boundary layer bleed (at the position of the cowl shock impingement and at the location of the smallest internal cross section height), the total pressure recovery can be improved significantly. However, the mass flow ratio is reduced by boundary-layer mass flow being removed by the bleed. Using multiple holes instead of a single slot for the bleed configuration further increases the total pressure recovery. Moreover, the slight decrease of the mass flow ratio at high levels of the exit pressure signals the near choking of the inlet, making control of the inlet easier.

Note that, by using boundary-layer bleed in a hypersonic inlet, the gain in total pressure recovery is linked with a reduction of the mass flow ratio. Therefore, the decision to implement bleed in an inlet should be based on the basic demands for the inlet system, which are in general maximum total pressure or maximum mass flow.

Conclusion

Methods for the manipulation of shock/boundary-layer interactions (with a focus on boundary-layer bleed) for the use in hypersonic inlets have been presented. To study the main parameters that influence boundary-layer bleed, fundamental investigations (numerical as well as experimental) have been carried out using generic models to isolate a single shock/boundary-layer interaction.

Favorable values for the most important boundary-layer bleed design parameters, that is, bleed slot width, bleed slot angle, and bleed slot position, have been characterized by performing experimental and numerical examinations using a generic flat plate model. It has been shown that boundary-layer bleed can be used very effectively for the control and reduction of shock-induced boundary-layer separations, as well as for the reduction of related, vortex-induced high local thermal loads.

To study the effects of the three-dimensional flowfield, the generic model has been equipped with a side wall. An analysis using infrared thermography has shown the effectiveness of boundary-layer bleed in this configuration, yielding recommendations for a proper bleed setup. Furthermore, the usefulness of bleed for the reduction of boundary-layer separations at compression ramps could be demonstrated.

Finally, the results of the investigations obtained with the generic models have been applied for the optimization of a hypersonic inlet model (using the bleed design parameters mentioned earlier). A significant increase of the inlet performance regarding the total pressure recovery could be proved. However, the use of boundary-layer bleed in a hypersonic inlet to control shock/boundary-layer interactions depends strongly on the basic demands of the inlet purpose, because a gain in total pressure recovery is often combined with a slight loss in inlet mass flow. The results of the investigations presented may, thus, give support for the design and the optimization of hypersonic inlets.

Acknowledgments

The studies presented in this paper, which have been carried out at the Institute for Fluid Mechanics, Wind Tunnel Division of the DLR, German Aerospace Research Center, are part of the Deutsche Forschungsgemeinschaft Sonderforschungsbereich 253 at the University of Aachen. The authors gratefully acknowledge the support by Deutsche Forschungsgemeinschaft and the German Aerospace Research Center.

References

[1] Koschel, W., Rick, W., and Rüggeberg, T., "Study of Flow Phenomena in High Speed Intakes," AIAA Paper 92-5029, Dec. 1992.

[2] Schulte, D., Henckels, A., and Schell, I., "Boundary Layer Bleed in Hypersonic Inlets," *New Results in Numerical and Experimental Fluid Mechanics—Contributions to the 10th DGLR/AG STAB Symposium*, Notes on Numerical Fluid Mechanics, Vol. 60, 1997, Vieweg, Brunswick, Germany, pp. 296–303.

[3] Schulte, D., Henckels, A., and Wepler, U., "Reduction of Shock Induced Boundary Layer Separation in Hypersonic Inlets Using Bleed," *Aerospace Science and Technology*, Vol. 2, No. 4, 1998, pp. 231–239.

[4] Henckels, A., Kreins, A. F., and Maurer, F., "Experimental Investigation of Hypersonic Shock/Boundary Layer Interaction," *Zeitschrift für Flugwissenschaften und Weltraumforschung*, Vol. 17, No. 2, 1993, pp. 116–124.

[5] Kreins, A. F., Henckels, A., and Maurer, F., "Experimental Studies of Hypersonic Shock Induced Boundary Layer Separation," *Zeitschrift für Flugwissenschaften und Weltraumforschung*, Vol. 20, No. 2, 1996, pp. 80–88.

[6] Kornilov, V. I., "Formation Peculiarities of the Flow Structure in a Corner Configuration under the Conditions of Interaction with the Impinging Incident Shock Wave," *Thermophysics and Aeromechanics*, Vol. 2, No. 2, 1995, pp. 95–104.

[7] Délery, J., "Shock/Shock and Shock-Wave/Boundary-Layer Interactions in Hypersonic Flows," Special Course on Aerothermodynamics of Hypersonic Vehicles, AGARD-R-761, 1988, pp. 9-1–9-51.